INSTITUTE OF PHYSICS PUBLISHING JOURNAL OF PHYSICS B: ATOMIC, MOLECULAR AND OPTICAL PHYSICS

J. Phys. B: At. Mol. Opt. Phys. **35** (2002) 1893–1907 PII: S0953-4075(02)33135-3

Projectile and target ionization in MeV u^{-1} collisions of Xe ions with N_2

R E Olson[1], R L Watson[2], V Horvat[2] and K E Zaharakis[2]

[1] Physics Department, University of Missouri-Rolla, Rolla, MO 65401, USA
[2] Cyclotron Institute and Department of Chemistry, Texas A&M University, College Station, TX 77843, USA

E-mail: olson@umr.edu

Received 24 January 2002, in final form 14 March 2002
Published 10 April 2002
Online at stacks.iop.org/JPhysB/35/1893

Abstract

Experimental cross sections are presented for single and multiple electron stripping from Xe^{18+} projectiles in collisions with N_2 at energies 2.0–9.3 MeV u^{-1}. The data are compared to 2–30 MeV u^{-1} n-body classical trajectory Monte Carlo calculations that explicitly include electrons on both centres. Two-centre electron–electron (e–e) and electron–screened nuclear interactions contribute to the ionization reactions. The computations are in reasonable accord for the total stripping cross section but underestimate the higher stages of multiple electron loss. An energy deposition model gives improved agreement with experiment. The energy dependence of the total stripping cross section is close to $E^{-0.5}$. Calculations are also presented for target ionization by Xe^{+}, Xe^{8+} and Xe^{18+} at 10 and 20 MeV u^{-1}. Projectile and target ionization cross sections are found to be comparable. Cross sections for projectile stripping by ionized targets are also calculated and found to be relatively insensitive to the ionization stage of the target. This latter observation is attributed to the compensating contributions between the two-centre e–e and electron–screened nuclear interactions.

1. Introduction

The subject of electron stripping from projectile ions by collision with atomic and molecular targets has been extensively investigated for several decades. Review articles document numerous sources of experimental data (see, for example, Allison (1958), Lo and Fite (1970), Dehmel *et al* (1973) and Tawara *et al* (1985)). However, there is very little information about stripping cross sections for low charge state, heavy ion projectiles in the 5–50 MeV u^{-1} energy range due to the limitations of available accelerators. At somewhat lower energies and moderate charge states, single and multiple projectile stripping cross sections are available for U^{10+} + H_2, N_2 at 1.4 MeV u^{-1} (Franzke 1981) and Xe^{11+}, Kr^{7+} + N_2 at 3.4 MeV u^{-1}

(Mueller *et al* 2001). For heavy ions near their equilibrium charge, there is an extensive set of measurements by Erb (1978) at 1.4 MeV u^{-1} for multiple stripping and electron capture from various gas targets. Additionally, Alonso and Gould (1982) have measured cross sections for single-electron capture and loss by highly charged Pb and Xe ions at 2.4, 4.6 and 8.4 MeV u^{-1}. However, no experimental data are available for low charge state heavy ions.

The current interest in projectile stripping cross sections for low charge state heavy ions in the 10–20 MeV u^{-1} range is prompted by the possibility of using heavy ions to initiate nuclear fusion in power generating reactors. In the USA, possible candidate ions for heavy ion fusion (HIF) are Rb^+, Cs^+, Xe^+ and Bi^+, with energies of 10–20 MeV u^{-1} (Meier 1998). Unfortunately, the low charges of these ions are far from their equilibrium values at these energies and no experimental data on stripping cross sections are available. Nevertheless, design data are needed to determine accelerator background pressure and pumping requirements. Moreover, questions arise concerning ion beam penetration and focusing in the reactor chamber where the background pressure is several mTorr due to the liquid Li based compound that is used to shield the reactor chamber walls from neutron damage. The Li compound is used to transport the heat generated in the deuterium–tritium (DT) nuclear fusion reactions to produce steam that drives electrical power generators.

Theoretical cross sections have been presented by Shevelko *et al* (1998, 2001) and Olson (2001) that indicate an unacceptable loss of the HIF beam in the reactor chamber due to stripping, which leads to space charge blowup with degraded focusing. The sets of calculations are independently based on the Born and classical trajectory Monte Carlo methods, respectively. A topic of critical interest is the energy dependence of stripping cross sections. Its establishment is important since near-term measurements on candidate HIF beams will be performed in the 1.4–3.6 MeV u^{-1} energy range (Stöhlker and DuBois 2001) and will need to be extrapolated to the higher energies of interest.

The present benchmark experiments with Xe^{18+} projectiles were conducted at the Texas A&M University Cyclotron Institute and are used to test calculations that employ an n-body classical trajectory Monte Carlo method that incorporates active electrons on both nuclear centres. In this paper we present experimental and theoretical stripping cross sections for collisions of Xe^{i+} with N_2. The experimental work is restricted to ions with $i = 18$ and covers the energy range of 2.0–9.3 MeV u^{-1}, while the theoretical calculations are performed for $i = 1$, 8 and 18 over the energy range from 2–30 MeV u^{-1}. Since, under intense beam conditions, it may be possible to self-neutralize the ion beam using electrons generated in ionizing collisions of the projectile with the target, target ionization cross sections are calculated as well. Furthermore, the background gas may be photoionized near the DT target in an HIF application, and therefore, we have estimated the stripping cross sections for projectiles colliding with ionized targets.

2. Experiment

Beams of 2.0 MeV u^{-1} Xe^{11+}, 3.4 MeV u^{-1} Xe^{16+} and 6.0, 8.0 and 9.3 MeV u^{-1} Xe^{18+} were extracted from the Texas A&M K500 superconducting cyclotron and directed through a bending magnet into the target chamber. In the case of the 2.0 MeV u^{-1} beam, it was necessary to employ a 10 μg cm^{-2} carbon stripping foil inserted in front of the bending magnet to obtain the desired charge state of 18^+. The 3.4 MeV u^{-1} beam was stripped from 16^+ to 18^+ by valving off one of the vacuum pumps in front of the bending magnet, thereby creating a relatively high pressure region in a small section of the beam line. Upon entering the target chamber, the beams passed through a series of four collimators, having diameters ranging from 1 to 3 mm, and on into a windowless, differentially pumped gas cell having an effective length of 2.08 cm.

After emerging from the gas cell, the beams passed between the poles of a charge dispersing magnet into a one-dimensional position-sensitive microchannel plate detector (PSD).

The N_2 target gas pressure was monitored using an absolute pressure transducer (MKS 627B Baratron) and the gas flow was regulated by an automated control valve (MKS 245) and a flow controller (MKS 244E) that maintained the pressure in the gas cell to within $\pm 0.6\%$ of the selected value over a pressure range of 0–64 mTorr. The PSD had an active length of 10 cm and width of 1.5 cm. It was attached to a moveable mount and could be remotely positioned in the vertical direction by activating a drive motor. Signals from the top and bottom of the resistive anode were shaped using conventional preamplifiers and amplifiers. The position signals, obtained by taking the ratios of the top signals to the sums of the top plus bottom signals, were processed using a personal computer-based multichannel analyser. In order to avoid rate-dependent gain shifts and pulse pile-up problems, counting rates were limited to around 1500 s^{-1}. A typical charge state spectrum is shown in figure 1 for 6 MeV u^{-1} Xe^{18+} ions with an N_2 pressure of 64 mTorr in the gas cell. Periodic checks were performed to ensure that the detection efficiency of the PSD remained uniform over the active region of the microchannel plates. This was accomplished by inserting a 10 μg cm^{-2} thick carbon foil in the beam path immediately behind the exit aperture of the gas cell and taking overlapping spectra of the resulting charge distribution at different positions along the entire length of the detector. During the accumulation of these spectra, the beam intensity was continuously monitored by accelerating the secondary electrons ejected from the carbon foil onto a microchannel plate electron detector. The root-mean-square deviation from the average relative efficiency along the plate never exceeded 5% in any of these checks.

Each charge state peak appearing in the position spectra of the projectile ions was integrated and divided by the total number of incident ions to obtain the corresponding fraction F_i of projectile ions in charge state i. The rate of change of charge fraction F_i as the projectile traverses a gas cell of length l containing gas atom density ρ is given by the well known rate equation

$$\frac{\mathrm{d}F_i}{\mathrm{d}\pi} = \sum_k F_k \sigma_{ki} - F_i \sum_j \sigma_{ij} \tag{1}$$

where $\pi = \rho l$ and σ_{mn} is the cross section for changing from charge m to charge n due to electron capture ($m > n$) or electron loss ($m < n$) in a collision. The solutions to this coupled set of equations are extremely complicated, but for low pressures where $\pi\sigma_{mn} \ll 1$, the individual charge fractions may be approximated by polynomials (McDaniel *et al* 1993, Vancura *et al* 1993):

$$F_i = a + b\pi + c\pi^2 + \cdots, \tag{2}$$

where $a = F_i(\pi = 0)$, $b = \sigma_i$ (cross section for changing from incident charge q to charge i in a single collision) and $c =$ products of cross sections for producing charge state i in double collisions.

The first term in equation (2) is the background fraction of ions in charge state i (i.e. the fraction of incident ions that change to charge state i as a result of collisions with the residual gas in the beamline). In the pressure range employed here, higher-order terms representing contributions from more than two collisions were negligible.

The cross sections for removing i electrons in *single* collisions with target gas atoms were determined using the growth-rate method (Tawara and Russek 1973). Charge fractions were measured at eight pressures covering the range from 0 to 64 mTorr and the resulting pressure dependence curves were fitted with second-order polynomials. The single-collision cross sections σ_i are (according to equation (2)) given by the coefficients of the linear terms.

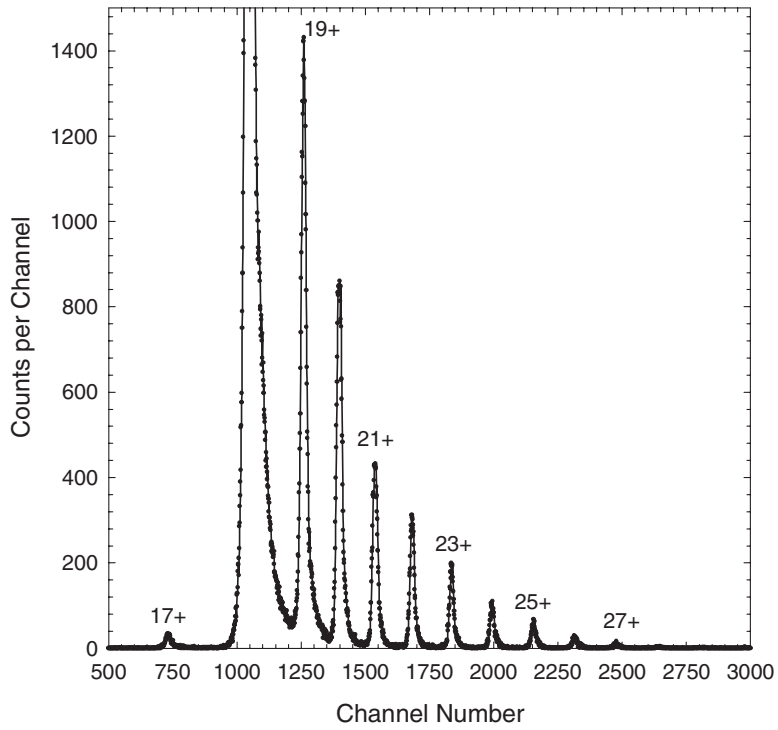

Figure 1. Charge distribution of 6 MeV u^{-1} Xe ions after passing through a gas cell containing 64 mTorr of N_2. The large peak that is off scale is due to the charge-unchanged beam (incident charge = 18^+).

Table 1. Experimental cross sections for single-electron capture and the loss of one to eight electrons for Xe^{18+} ions colliding with nitrogen (10^{-18} cm^2/atom).

Reaction	2.0 MeV u^{-1}	3.4 MeV u^{-1}	6.0 MeV u^{-1}	8.0 MeV u^{-1}	9.3 MeV u^{-1}
1-capture	6.9 ± 1.0	1.84 ± 0.19	0.397 ± 0.043	0.139 ± 0.024	0.091 ± 0.011
1-loss	19.2 ± 2.9	16.4 ± 1.7	13.1 ± 1.3	11.1 ± 1.2	10.7 ± 1.0
2-loss	7.1 ± 1.1	7.30 ± 0.76	7.18 ± 0.70	6.53 ± 0.66	6.28 ± 0.60
3-loss	3.99 ± 0.55	3.51 ± 0.35	2.96 ± 0.29	2.42 ± 0.24	2.06 ± 0.20
4-loss	2.70 ± 0.40	2.33 ± 0.24	1.87 ± 0.19	1.41 ± 0.14	1.22 ± 0.12
5-loss	1.86 ± 0.26	1.67 ± 0.17	1.04 ± 0.11	0.748 ± 0.078	0.588 ± 0.058
6-loss	1.19 ± 0.22	0.97 ± 0.10	0.556 ± 0.061	0.383 ± 0.041	0.293 ± 0.030
7-loss	0.65 ± 0.13	0.523 ± 0.056	0.276 ± 0.033	0.203 ± 0.025	0.138 ± 0.015
8-loss	0.265 ± 0.053	0.219 ± 0.029	0.108 ± 0.018	0.0894 ± 0.0147	0.0543 ± 0.0074
Total loss	37.0 ± 3.2	32.9 ± 1.9	27.1 ± 1.5	22.9 ± 1.4	21.4 ± 1.2

A representative set of growth curves measured for 6 MeV u^{-1} Xe^{18+} ions are shown in figure 2. Cross sections for the loss of one to eight electrons are presented in table 1. The indicated errors take into account uncertainties in the effective cell length (2%), absolute pressure measurement (5%), peak integration and counting statistics.

The validity of the approximation used to extract the experimental cross sections (i.e. equation (2)) in the present application was tested by assuming a reasonable set of charge changing cross sections and calculating the growth curves for one to eight electron loss and

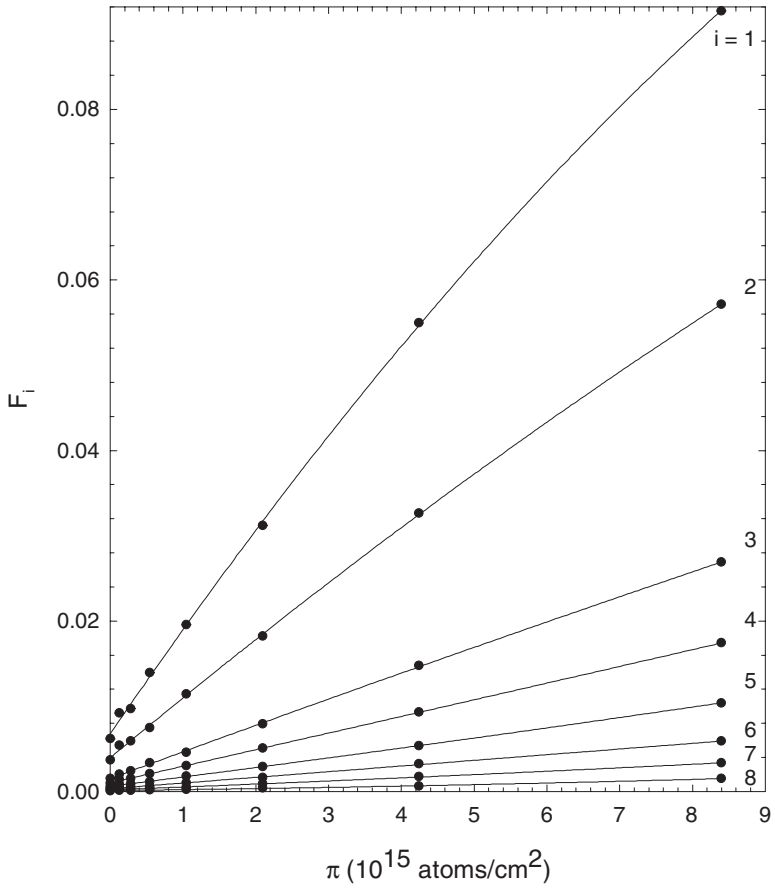

Figure 2. Pressure dependence of the charge fractions for one to eight electron loss in collisions of 6 MeV u^{-1} Xe^{18+} with N_2. The curves show the results of least squares fits to second-order polynomials.

one to three electron capture via numerical solution of the rate equations (equation (1)). Then the calculated growth curves were fitted with second-order polynomials over the pressure range of 0–100 mTorr. For the electron loss curves, the largest difference between the value of the linear coefficient of the polynomial fit and the corresponding (assumed) cross section was 6%, which occurred for the one-electron loss case. The deviations for all of the multiple-loss cross sections were less than 1%. In addition, it was found that the agreement improves rapidly as the pressure range is decreased. For larger pressure ranges, good agreement is obtained by increasing the polynomial to third order.

3. Theory

The calculation of electron loss from dressed projectiles at high energies must include both the electron–electron (e–e) and screened nuclear–electron (N–e) interactions between nuclear centres. In the case of stripping from Xe^{18+} projectiles, individual target electrons have sufficient energy in the rest frame of the projectile to ionize the ion at collision energies above approximately 1 MeV u^{-1}, since the equivalent electron energy at this velocity is

approximately 550 eV. For lower charge state ions, the e–e interactions become even more important. Screening (N–e interaction) and anti-screening (e–e interaction) models were initially developed by McGuire *et al* (1981) and Anholt (1986) using the Born approximation. These two collision mechanisms have completely different dynamical signatures (Fiol *et al* 2001, Kollmus *et al* 2001). In general, the screening (N–e) interaction dominates in hard, small impact parameter collisions, while the anti-screening (e–e) interaction dominates the large impact parameter collisions. Calculations must encompass the effects of both the e–e and N–e interactions in order to provide reasonable results.

Important to our discussion is a clear definition of the terms (N–e) and (e–e) interactions. What we term e–e interactions are those that directly contribute to the ionization cross sections via dynamical interactions of the electrons between nuclear centres. The N–e events are interactions between the electrons attached to one centre and the screened nuclear charge on the other centre. Thus, it is important to note that the e–e interaction potential in the Hamiltonian has two contributions; one of screening the nuclear charge and the other of dynamically inducing ionization events via binary collisions between the electrons on the two nuclear centres.

From a theoretical point of view, the complexity of the problem arises mainly due to the large number of interactions involved, which increases as $(n^2 - n)/2$, where n is the number of particles. In the nCTMC calculations performed here, we have neglected the e–e interactions between target and projectile electrons on the same centre and have incorporated this correlation by using simple static screened interactions between nuclei and each of their electrons (Olson *et al* 1989). With this simplification, the number of significant interactions decreases significantly. It is worth noting, however, that the relevant ionizing interactions, i.e. those between particles on the two centres, are considered in an exact way. Thus, the Hamiltonian for the nCTMC method is written as

$$H = (H_o + V_{NP-eP} + V_{NT-eT}) + V_{NP-NT} + V_{NT-eP} + V_{NP-eT} + V_{eP-eT} \qquad (3)$$

where H_o is the kinetic energy and the potential interaction subscripts are denoted by NP (nucleus projectile), NT (nucleus target), eP (electron projectile) and eT (electron target). The terms in the parentheses in equation (3) describe the separate centres that do not produce transitions. It is well known that the internuclear interaction does not contribute significantly to the total cross sections since the nuclei do not exchange a large amount of energy. The simultaneous ionization of both centres is produced by the combined and competing N–e and e–e interactions.

The n-body CTMC calculations were computer intensive. For every system, all seven K- and L-shell electrons were included on the N-atom centre. Note: we make the usual assumption that the molecular properties of the nitrogen target have no effect on the stripping cross sections. This approximation is valid at high projectile energies because of the relatively small effect molecular binding has on the electron ionization energies. For the Xe^{i+} projectile, we utilized 17–18 electrons leading to 26- or 27-body calculations, respectively. Specifically, the electrons included are $Xe^{+}(4d^{10}5s^{2}5p^{5})$, $Xe^{8+}(4s^{2}4p^{6}4d^{10})$ and $Xe^{18+}(3d^{10}4s^{2}4p^{6})$. The respective core electrons are considered inactive and completely screen the nucleus. Since the nCTMC calculations follow the x, y and z positions and their conjugate momenta of each particle, the number of coupled equations required to determine the time evolution of each trajectory was 156 and 162, respectively. Runs with smaller basis sets on the Xe^{i+} were made to verify convergence in the cross sections for up to five-fold ionization of the projectile.

As is usual for CTMC calculations, ionization and capture are determined from the binding energies of the electrons relative to both centres. Because of the high binding energies of the electrons initially bound to the projectile, as compared to those electrons on the target, even one

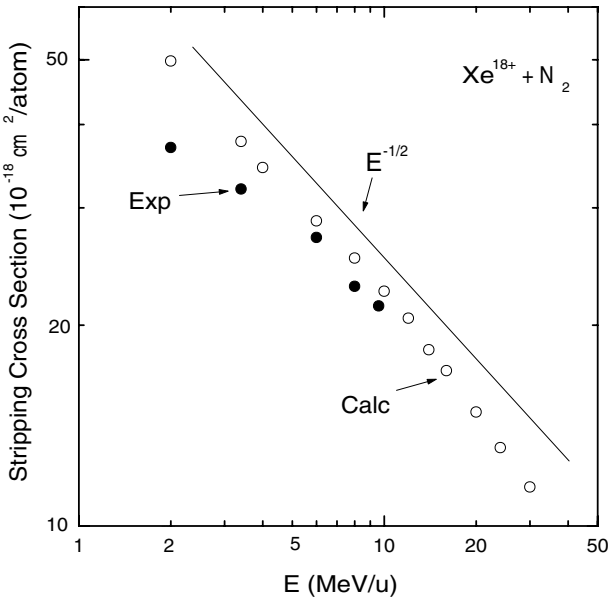

Figure 3. Total projectile stripping cross sections (cm^2/atom) for Xe^{18+} + N_2 collisions. Experimental results are displayed by full circles and the calculations by open circles.

electron stripping from the projectile was concomitant with multiple electron removal from the target. At the lower energies where electron capture is significant, this n-body aspect of the collision leads to difficult bookkeeping problems as the electron removal from each nucleus gives rise to both ionization and electron capture between centres. Thus, a seemingly simple calculation, such as single capture or ionization, is, in reality, a complicated n-body problem.

4. Results

The cross section most needed for planning and designing an HIF nuclear reactor is that for the overall total projectile stripping. Stripping cross sections determine the accelerator vacuum requirements and the focusing to the DT pellet in the reactor chamber. We first present those for the Xe^{18+} reaction:

$$Xe^{18+} + N_2 \rightarrow Xe^{i+} + \cdots, \qquad i > 18. \tag{4}$$

In figure 3, the calculated values are compared to experimental results. In general, except at the lowest energy of 2 MeV u^{-1} where electron capture complicates the calculations, the agreement is reasonable and better than 20%. Note, we have presented the cross sections in terms of cm^2/atom. The cross section for the N_2 molecule itself is two times the value given.

The energy dependence is quite surprising. We had expected an E^{-1} dependence since that is what is predicted by the binary encounter theory, with the Born approximation yielding $E^{-1} \ln E$ in the high energy limit. A line showing a $E^{-0.5}$ scaling dependence is shown in figure 3. We attribute this much slower energy dependence to the multi-electron character of the stripping collisions. At each collision energy there is always an electron sub-shell that has optimum probability for ionization, resulting in a slower energy dependence than predicted by one-electron models. Note also that the cross sections are quite large, greater than 10^{-17} cm^2, even for a relatively high charge state of 18^+.

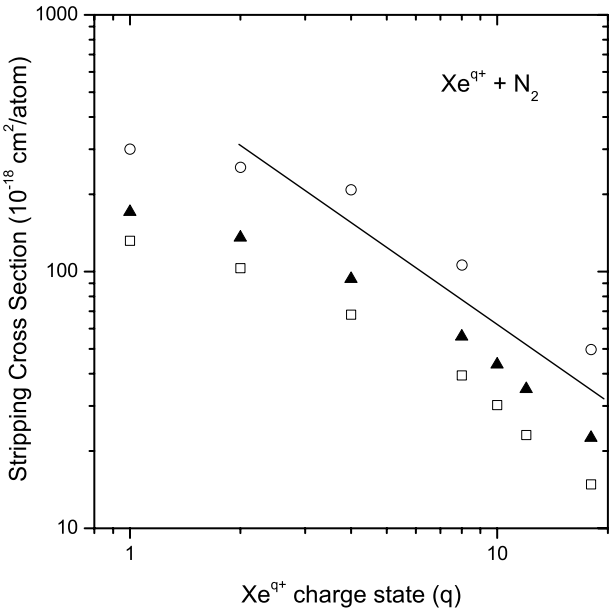

Figure 4. Calculated total projectile stripping cross sections as a function of incident charge state for Xe^{q+}+ N_2 at 2 MeV u^{-1} (open circles), 10 MeV u^{-1} (full triangles) and 20 MeV u^{-1} (open squares). The full line indicates a q^{-1} dependence.

In figure 4 the calculated total stripping cross sections as a function of incident charge state, $q = 1$–18, for 2, 10 and 20 MeV u^{-1} projectiles are given. Evidently, there is no simple charge state dependence for the stripping cross sections that includes the lowest incident charge states. For charges above about 5^+, the calculated cross sections vary roughly with the inverse of the charge state. A decrease with incident charge is expected since the energy required to ionize an electron from the projectile increases with q.

For the lowest projectile charges, we find the stripping cross sections become almost independent of charge state. This reflects a saturation of ionization probability as the cross section for $q = 1^+$ approaches the geometric value of 4.8×10^{-16} cm^2 obtained from the radial expectation value of the outer (5p) electrons. In fact, the 2 MeV u^{-1} cross sections are all very close to their geometric value, which is 6.7×10^{-17} cm^2 for 8^+ and 5.3×10^{-17} cm^2 for 18^+.

One-electron theories, such as the binary encounter and first Born approximation, predict that the electron loss cross section should be inversely proportional to the ionization potential (IP) of the active electron. Such a comparison is displayed in figure 5. The calculations show a slower dependence on the IP of the outer electron for each projectile ion than that given by the IP^{-1} line on figure 5. As in the q dependence of figure 4, such a difference from first-order theories is a reflection of the n-body nature of these collisions. In principle, any scaling law should include the number of active electrons participating in the ionization process. However, this estimation is difficult even within a given sub-shell since the individual ionization energies vary greatly.

For HIF applications, where the target region can be at very high temperatures, one must consider the fact that the target atoms will be photoionized. Also, for multi-pulsed intense beam applications the target can also be collisionally ionized by a preceding ion beam pulse. Thus, we present projectile stripping cross sections for

$$Xe^{q+} + N^{j+} \rightarrow Xe^{i+} + \cdots, \tag{5}$$

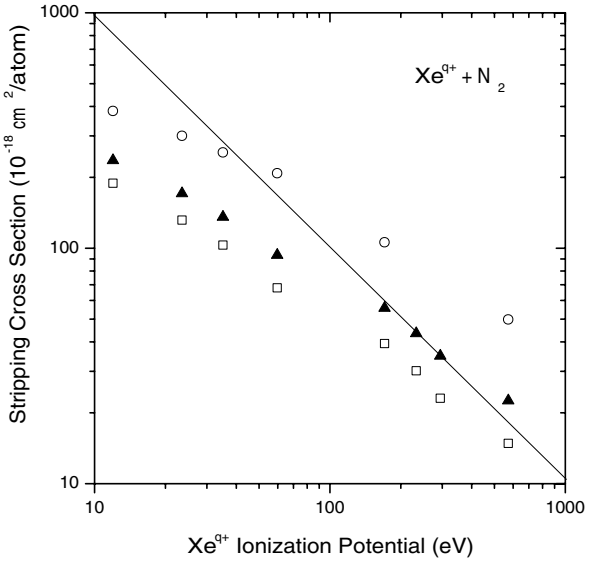

Figure 5. Cross sections of figure 4 plotted against the first IP of Xe^{q+}. The full line indicates an inverse dependence on IP.

for Xe^{+}, Xe^{8+} and Xe^{18+} projectiles and charge states of the nitrogen target from neutral to fully ionized. This calculation was accomplished within the nCTMC method simply by sequentially removing one electron from the N centre and repeating the *n*-body calculations. Cross sections were computed for collision energies of 10 and 20 MeV u^{-1}.

The results for ionized targets are presented in figure 6. Interestingly, we find that the stripping of the 8^{+} and 18^{+} ions changes very little with the stage of ionization of the target. For the 1^{+} case the cross section only increases by about a factor of three from neutral nitrogen to the fully stripped 7^{+} case. These results are surprising since first-order theories predict that the cross section should simply increase with the square of the target charge. However, such a prediction assumes the target is fully stripped and devoid of electrons. We must remember that at these energies the target electrons have sufficient energy in the rest frame of the projectile to ionize it. Thus, a proper description for the projectile stripping must include the dynamic e–e collisions between centres (e–e interactions) along with collisions of the screened target nucleus with the projectile electrons (N–e interactions). For the 8^{+} and 18^{+} projectile ions, increasing the charge state of the target effectively decreases the number of active e–e interactions, but this effect is counteracted by the decreased screening of the nuclear charge. For 1^{+} ions, the increase in the target nuclear charge more than compensates for the loss of the e–e interactions, while Xe^{18+} even shows a slight decrease in the stripping cross section until the K-shell electrons of the N target are removed.

Besides the electron stripping from the projectile, at low energies electron capture can also contribute significantly to projectile charge change. Therefore, we consider the reaction

$$Xe^{18+} + N_2 \rightarrow Xe^{17+} + \cdots. \tag{6}$$

In general, electron capture cross sections decrease rapidly for impact velocities higher than the orbital velocity of the target electrons. For nitrogen, the L-shell electrons will be relatively inactive to electron capture at MeV u^{-1} energies. However, the K-shell electrons have velocities of 6–7 au, which correspond to a projectile energy of about 1 MeV u^{-1}. Thus, one would expect the K-shell electrons of nitrogen to dominate the electron capture reaction at energies above 1 MeV u^{-1}.

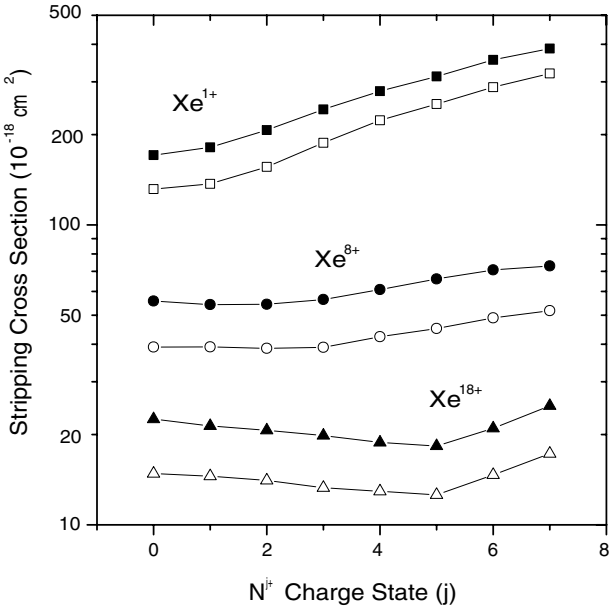

Figure 6. Calculated total projectile stripping cross sections for Xe^{q+}, $q = 1$, 8 and 18, as a function of the initial charge state of an N^{j+} target. The full symbols are for 10 MeV u^{-1} and the open symbols are for 20 MeV u^{-1}.

In figure 7 we present the experimental and theoretical single-electron capture cross sections for Xe^{18+}. The theoretical values overestimate the data by approximately a factor of two. At 2 MeV u^{-1} the capture cross sections are within a factor of four of the total stripping cross sections shown in figure 3, implying that the two processes are competing with each other. Moreover, we find that electron capture to the projectile and projectile stripping are active in the same impact parameter range. Most of the electron capture occurs simultaneously with stripping, resulting in a high fraction of projectile overall electron loss rather than gain. Thus, calculation of the capture cross section is dependent not only on the probability for electron transfer from the target to projectile, but also on the probability of projectile electron loss to the continuum. What appears to be a simple one-electron transfer reaction is seriously complicated by projectile stripping occurring concurrently, resulting in calculated values of poor accuracy.

Also given in figure 7 are the recoil charge states of the N atom coincident with single-electron capture. We find that recoil ion charge states 5^+, 6^+ and 7^+ dominate, implying that capture is primarily from the K-shell with some contribution from the 2s level.

For some applications, such as beam neutralization schemes involving intense ion beams, it is important to have knowledge of the total electron production from both the projectile and the target. For this reason, we present calculations of the target ionization for

$$Xe^{q+} + N \rightarrow \cdots + N^{i+}, \tag{7}$$

as a function of the recoil ion charge state i^+ and for projectile charges q from 1^+ to 18^+. The results for 10 and 20 MeV u^{-1} projectiles are presented in figures 8 and 9, respectively. Note that the curve labelled 'total' is simply the sum of the partial cross sections for leaving the nitrogen atom in any charge state i.

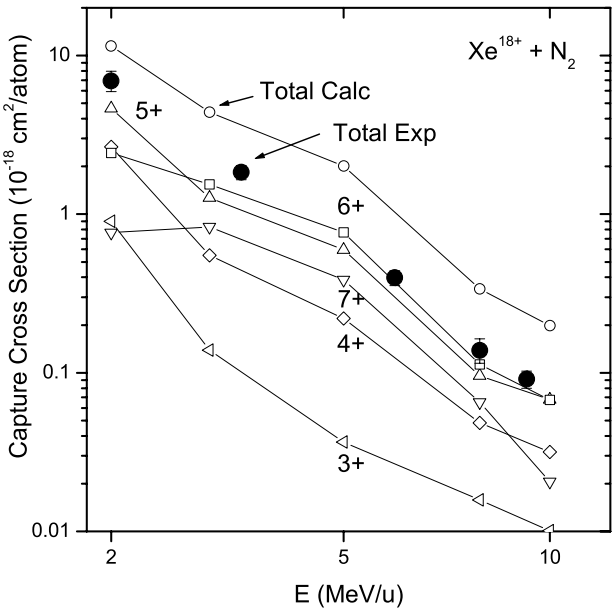

Figure 7. Single-electron capture cross sections for $Xe^{18+}+N_2$ collisions. The full circles show the experimental values, while the open circles show the calculated cross sections. The other symbols denote calculated coincident cross sections for single capture with the N atom left in the fully stripped 7^+ state (open inverted triangles), 6^+ state (open squares), 5^+ state (open triangles), 4^+ state (open diamonds) and 3^+ state (rotated triangles).

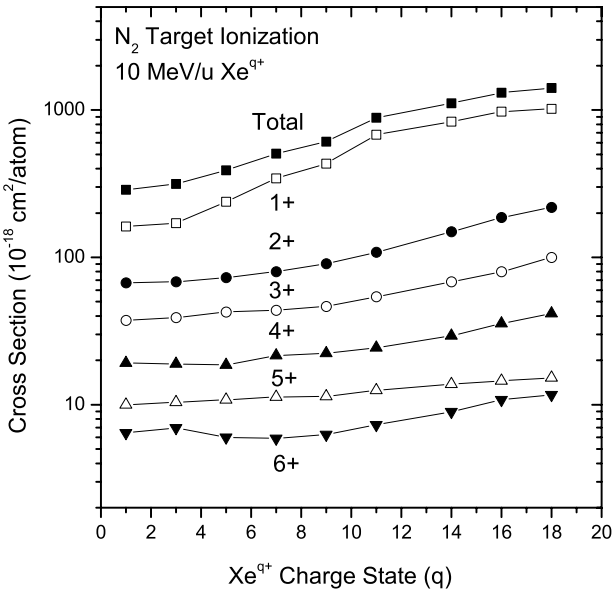

Figure 8. Calculated total-, single- and multiple-electron loss cross sections from the N_2 target by 10 MeV u^{-1} impact of Xe ions in incident charge states from 1^+ to 18^+.

Two observations are readily apparent. First, the overall total cross section increases much slower than the q^2 dependence predicted by first-order theories for fully stripped projectile ions.

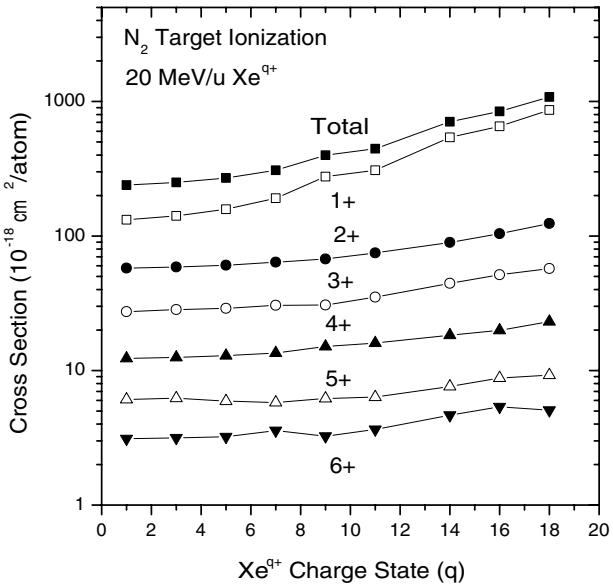

Figure 9. Same as figure 8 but for 20 MeV u^{-1} Xe ion impact.

Second, the energy dependence is much slower than an expected E^{-1}. We attribute both of these dependences to the fact that the projectile ions are not fully stripped. The target electrons are removed by a combination of e–e and N–e interactions between nuclear centres, just as in the case of projectile stripping. For 1^+ projectile ions, the projectile stripping and the target ionization cross sections are comparable. For higher projectile charge states, the target ionization cross sections greatly exceed those for projectile stripping. In all cases, multiple ionization of the target makes an appreciable contribution to its total electron removal cross section.

For an accurate prediction of the charge state evolution of a fast projectile passing through a thick target, it is essential to know not only the overall total stripping cross section, but also its single- and multiple-electron removal cross section components. This is because higher charge states may be reached more quickly via a single collision that leads to multiple-electron loss rather than through a series of single-electron removal collisions.

The experimental and theoretical stripping cross sections for the removal of one to eight electrons from Xe^{18+} are presented in figure 10. As expected from the early work of Erb (1978) and others, there is considerable multiple-electron removal from the projectile at these energies. It is also apparent that the nCTMC calculations, which include the correct binding energies for multiple ionization, are only qualitatively reliable for predicting cross sections for the loss of one to three electrons. Moreover, even when all 18 electrons on the projectile were included in the calculation, convergence of the stripping cross sections could be verified only up to five-fold loss. Differences between theory and experiment are of the order of 50% for three-fold ionization. For the higher multiplicities of electron loss, not only are the absolute values of the calculated cross sections in error, but they also decrease with increasing projectile energy much more rapidly than the experimental cross sections. Our theoretical values behave as would be expected from an independent electron model where the n-fold ionization probability is roughly proportional to P^n, where P is the probability of single-electron removal. Although there are marked differences between the theoretical and experimental n-fold loss cross sections, the overall total cross sections are in reasonably good agreement, with the largest discrepancy being 35% at 2 MeV u^{-1}. This indicates at least the range of interaction is correctly portrayed.

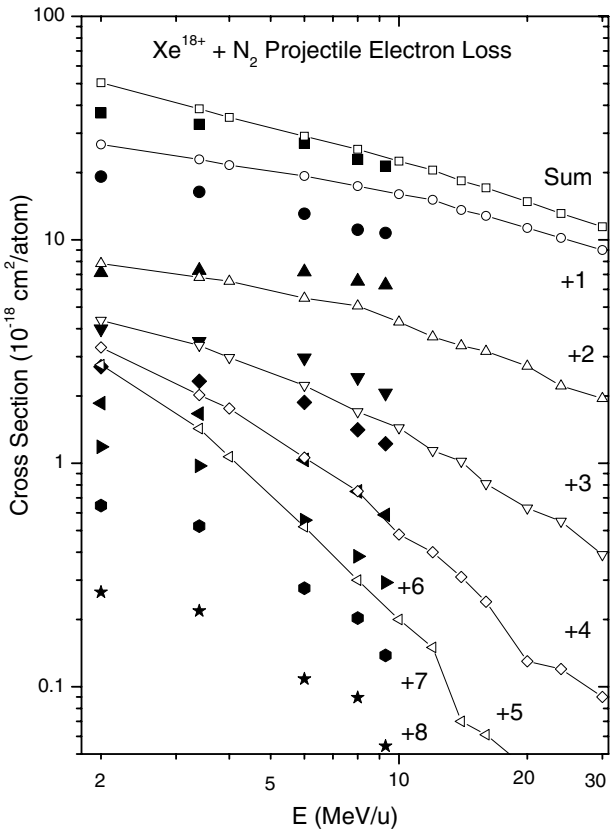

Figure 10. Single and multiple stripping cross sections for $Xe^{18+} + N_2$ collisions. The experimental data are given by full symbols and the calculations using a direct ionization model are displayed by open symbols.

The comparison with experiment in figure 10 indicates that our direct ionization model is not capable of reliably predicting the differential cross sections. One source of ionization that is not accounted for in the standard nCTMC method is the decay of projectile excited states via Auger transitions. Using the present benchmark data, it is possible to test another theoretical method for predicting stripping cross sections—the energy deposition model. In the energy deposition model, one simply compares the collisional energy deposited to the excited ion with the experimental IPs for sequential ionization.

A merit of the nCTMC method is that the post-collision projectile excitation is readily available without further approximation. The energy deposition model yields an upper limit to the multiple stripping cross sections since it assumes complete Auger decay of the excited ion. The results of the energy deposition model calculations are compared with experiment in figure 11. The combination of direct ionization with the energy deposition model displays improved agreement with experiment, indicating that collisional excitation of the ion with subsequent Auger decay makes an important contribution to projectile multiple ionization. Agreement with experiment on this difficult n-body problem is now acceptable, with the maximum difference on the overall total cross section being 17% at 2 MeV u^{-1}. Moreover, the magnitudes and energy dependences of the differential cross sections are now in reasonable accord.

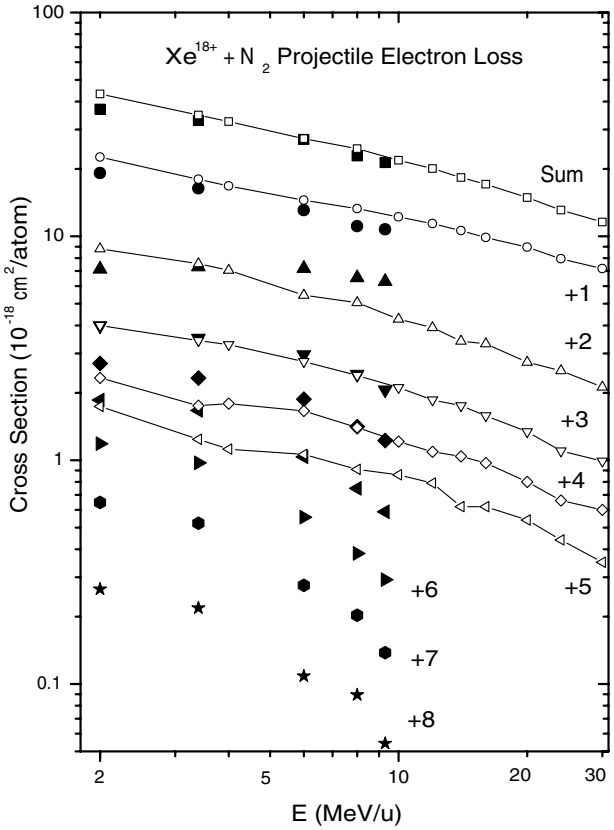

Figure 11. Experimental single and multiple stripping cross sections for $Xe^{18+} + N_2$ compared to calculated results obtained using the energy deposition model.

5. Conclusions

Projectile stripping of Xe^{q+}, $q = 1$–18, ions by N_2 was investigated at energies from 2–30 MeV u^{-1}. Theoretical 26- and 27-body nCTMC calculations were compared to experimental data for the Xe^{18+} ion. The overall total cross sections are in reasonable agreement with one another. However, an energy deposition model must be incorporated in order for the stripping cross sections differential in projectile electron loss to be in reasonable agreement with experiment. For all systems, the energy and projectile charge dependences of the cross sections are far removed from predictions based on one-electron models for fully stripped ions. This is due to the competing behaviour of the e–e and screened N–e interactions.

Electron capture and target ionization cross sections are also presented. In both cases there are numerous multiple electron transitions. Even single capture proceeds with the concurrent removal of 5–7 electrons from the target. Electron capture is an especially difficult theoretical problem. This is because capture occurs simultaneously with strong projectile stripping.

A surprising result was the behaviour of the theoretical stripping cross sections for ionized targets. We had expected the cross sections to increase rapidly with increasing target charge, but in fact little increase was observed. This is attributed to the compensating changes in the e–e and screened N–e contributions.

Acknowledgments

We thank George Kim for his patient and skillful work on the beam optics, and Yong Peng and Anna Allred for help with some of the measurements. This research was supported by the Robert A Welch Foundation and the DOE Office of Fusion Energy Sciences.

References

Allison S K 1958 *Rev. Mod. Phys.* **30** 1137
Alonso J and Gould H 1982 *Phys. Rev.* A **26** 1134
Anholt R 1986 *Phys. Lett.* A **114** 126
Dehmel R C, Chau H K and Fleischmann H H 1973 *At. Data* **5** 231
Erb W 1978 *GSI Report* GSI-P-78, Darmstadt
Fiol J, Olson R E, Santos A C F, Sigaud G M and Montenegro E C 2001 *J. Phys. B: At. Mol. Opt. Phys.* **34** L503
Franzke B 1981 *IEEE Trans. Nucl. Sci.* **28** 2116
Kollmus H, Moshammer R, Olson R E, Hagmann S, Schulz M and Ullrich J 2002 *Phys. Rev. Lett.* **88** 103202
Lo H H and Fite W L 1970 *At. Data* **1** 305
McDaniel E W, Mitchell J B A and Rudd M E 1993 *Atomic Collisions—Heavy Particle Projectiles* (New York: Wiley)
McGuire J H, Stolterfoht N and Simmony P R 1981 *Phys. Rev.* A **24** 97
Meier W R 1998 *UCRL-JC*-130954
Mueller D, Grisham L, Kaganovich I, Watson R L, Horvat V and Zaharakis K E 2001 *Phys. Plasmas* **8** 1753
Olson R E 2001 *Nucl. Instrum. Methods* A **464** 93
Olson R E, Ullrich J and Schmidt-Böcking 1989 *Phys. Rev.* A **39** 5572
Shevelko V P, Böhne D and Stöhlker Th 1998 *Nucl. Instrum. Methods* A **415** 609
Shevelko V P, Tolstikhina I Yu and Stöhlker Th 2001 *Nucl. Instrum. Methods* B **184** 295
Stöhlker Th and DuBois R D 2001 private communication
Tawara H, Kato T and Nakai Y 1985 *At. Data Nucl. Data Tables* **32** 235
Tawara H and Russek A 1973 *Rev. Mod. Phys.* **45** 178
Vancura J, Marchetti V J, Perotti J J and Kostroun V O 1993 *Phys. Rev.* A **47** 3758